Geomechanics and Engineering, *Vol. 28, No. 3 (2022) 283-298*
https://doi.org/10.12989/gae.2022.28.3.283

The July 2, 2017, Lantian landslide in Leibo, China: mechanisms and mitigation measures

Kun He[1], Guotao Ma*[1,2], Xiewen Hu[1,3], Bo Liu[1] and Mei Han[4]

[1]*Faculty of Geosciences and Environmental Engineering, Southwest Jiaotong University, Sichuan Chengdu, China*
[2]*School of Engineering, University of Warwick, Coventry, United Kingdom*
[3]*Engineering Laboratory combined with national and local of spatial information technology of high-speed railway operation safety, Southwest Jiaotong University, Sichuan Chengdu, China*
[4]*School of Mathematics, Southwest Jiaotong University, Sichuan Chengdu, China*

(Received May 6, 2020, Revised December 5, 2021, Accepted December 8, 2021)

Abstract. Landslides triggered by the combination of heavy precipitation and anthropological disturbance in hilly areas cause severe damage to human lives, properties, and infrastructure constructions. A comprehensive investigation of the influencing factors and failure mechanisms of landslides are significant for disaster mitigation and prevention. This paper utilized the combination of detailed geological investigation, physical experimental testing as well as numerical modelling to determine the failure mechanism, and proposed a countermeasures of the Lantian landslide occurred on 2, July 2017. The results reveal that the Lantian landslide is a catastrophic reactivated slide which occurred in an active tectonic region in Southwest China. Because of the unique geological settings, the fully to highly weathered basalts in the study area with well-developed fractures favored the rainwater infiltration, which is the beneficial to slide reactivation. Engineering excavation and heavy precipitation are the main triggering factors to activate the slide motion. Two failure stages have been identified in the landslide. The first phase involves a shallow mass collapse originated at the upper slopes, which extends from the road to platform at rear part, which is triggered by excavation in the landslide region. Subjected to the following prolonged rainfall from 19 June to 2 July, 2017, the pore water pressure of the slope continually increased, and the groundwater table successively rise, resulting in a significant decrease of soil strength which leads to successive large-scale deep slide. Thereinto, the shallow collapse played a significant role in the formation of the deep slide. Based on the formation mechanisms of the landslide, detailed engineering mitigation measures, involving slope cutting, anchor cable frame, shotcrete and anchorage, retaining wall and intercepting ditch were suggested to reduce the future failure risk of the landslide.

Keywords: excavation; landslide; mitigation measures; numerical simulation; rainfall

1. Introduction

The Emeishan Large Igneous Province (ELIP) of China lies in the southwestern China, between Yangtze Craton to the east and the Tibetan Plateau to the west (Xu *et al*. 2001, Ali *et al*. 2005). The ELIP covers an area of $3\sim5\times10^5$ km^2 and the hillsides in this area are mainly composed of Emeishan basalts. In terms of the high strength, modulus and strong weathering resistance of basalts, the natural or engineering slopes composed of this type of rocks are often characterized by steepness and huge thickness. However, this area often are subjected strong tectonic movement and intense weathering, as a result, basalt rock mass has fractured properties (Ren *et al*. 2018), involving three types of preexisting weak structural surfaces or zones within the basalt rock mass, namely (1) primary structural planes; (2) tectonic structural planes; and (3) hypergenic structural planes, evidencing intense control of the landslides by geological structures. This character makes it vulnerable to failure when under the role of rainfall (Guo *et al*. 2020), blasting (Ma *et al*. 2018, Wang *et al*. 2021), or earthquake shock (Shen *et al*. 2018). There have been several catastrophic large-scale landslides in the Emeishan basalt area. For instance, the Lannigou landslide on 22 November 1965 in Luquan County, Yunnan Province, the southwest of China, resulted in fatalities of 444, blocking the Baishui River for half a year (Cheng *et al*. 2015). In 1991, a fatal landslide (called Touzhai landslide) suddenly occurred on the upslope of Touzhai gully located on the Panhe area, Yunnan, and 116 people were killed (Xing *et al*. 2015). On July 27, 2010, a complicated rock avalanche-mud flow induced by torrential rainfall in Hanyuan, Sichuan, burying 5 houses and causing 20 fatalities (Xu *et al*. 2011). A rainfall-induced reactivated ancient basalt landslide occurred in Yanyuan County, China, on July 19, 2018, resulting in 186 houses damages (He *et al*. 2021a, b). Further, a basalt landslide occurred in Jichang Town, Guizhou Province, resulting in 42 fatalities (Li *et al*. 2020).

In recent years, road excavation-induced landslides in mountainous areas continues to increase due to changes in land use, particularly in the underdeveloped area (Wen *et al*. 2004, Kainthola *et al*. 2015, Xue *et al*. 2018, Froude and Petley 2018, Peng *et al*. 2018, Ma *et al*. 2021a). During the formation of the cutting slope, owing to the redistribution of the stress resulting from excavation, the rock mass of the slope will undergo different deformation, even develop into

*Corresponding author, Research Fellow
E-mail: maguotao46@yahoo.com

ISSN: 2005-307X (Print), 2092-6219 (Online)

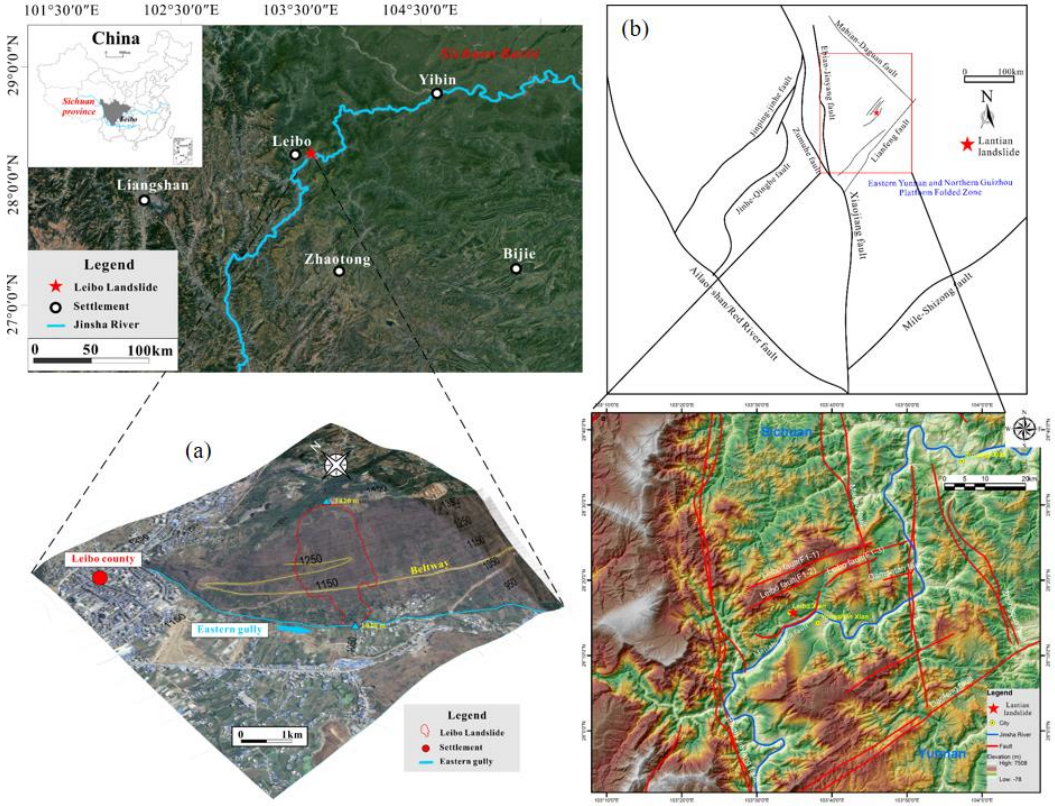

Fig. 1 (a) Geographical location of the Lantian landslide and (b) Tectonic map of the of the study area

failure under favorable conditions (Abderahman 2006, Huang 2009, Hu *et al*. 2013, Wang *et al*. 2013, Luo *et al*. 2017). Especially, rainfall is considered as one of the main triggering factors which can dramatically aggravate the deformation of cutting slopes (Crosta 2003, Kang *et al*. 2009, Lin *et al*. 2017, He *et al.* 2021c). In order to identify the future risk of slope failure, the formation mechanisms should be clarified. Numerical simulation provides an effective approach for this purpose. To date, these methods have made significant contributions to landslide studies. The SEEP/W module in the Geo-studio software is often performed to analyze the hydrological response of slopes during rainfall. SEEP/W uses a two-dimensional Richard equation to calculate pore water pressure variation (Acharya *et al*. 2014, 2015). Most recently, a finite element method, the Plaxis 2D software coupled with the strength reduction method has been developed to assess the stability state of slopes (Fawaz *et al*. 2014), and many studies have validated that the finite element method with the use of Plaxis 2D can be helpful for geological engineers defining appropriate mitigation measures (Schweiger *et al*. 2018, Nguyen *et al*. 2019, Khalifa *et al*. 2020).

In this paper, we carried out a typical road excavation and rainfall-induced landslide as a case study, namely Lantian landslide (He *et al*. 2019). This landslide can provide a well example for landslide-prone conditions in mountainous areas in China. Field investigations were performed to acquire landslide characteristics. Soils and rocks were sampled from in situ and conducted the laboratory tests to obtain geotechnical parameters. Boreholes were drilled in the slope to determine the sliding surface of the landslide. Numerical simulation based on Geo-studio software was applied to clarify the deformation characteristics contributing to road excavation and rainfall, respectively. Using the Plaxis 2D, a comprehensive failed slope mitigation measure is proposed. This study can improve the understanding of mechanisms of road excavation and rainfall-induced landslides and provide a suitable reference for design the mitigation measures in the road system in China.

2. Study area

The study area is located at Leibo County, Southwest Sichuan Province (Fig. 1). The highest elevation in the study area is 1470 m, while the lowest elevation is the Jinsha River of 385 m. The landform in the area is characterized by valley surrounded by mountains. The slope of this area ranges from 20°-35° and local slopes reach 50-70°. A beltway of Leibo County was built in the eastern slope, 1.1 km away from the County town. On 2 July 2017, a large-scale landslide took place at the beltway section in the Lantian Village, east of Leibo County (Fig. 1).

The study area is located in the north section of the Eastern Yunnan and Northern Guizhou Platform Folded Zone, along the east of the Sichuan-Yunnan rhombic fault block (Fig. 1(b)), which was formed through compression during Cenozoic collision between the Eurasian and Indian plates (Zhang *et al.* 1988), with the west boundary of

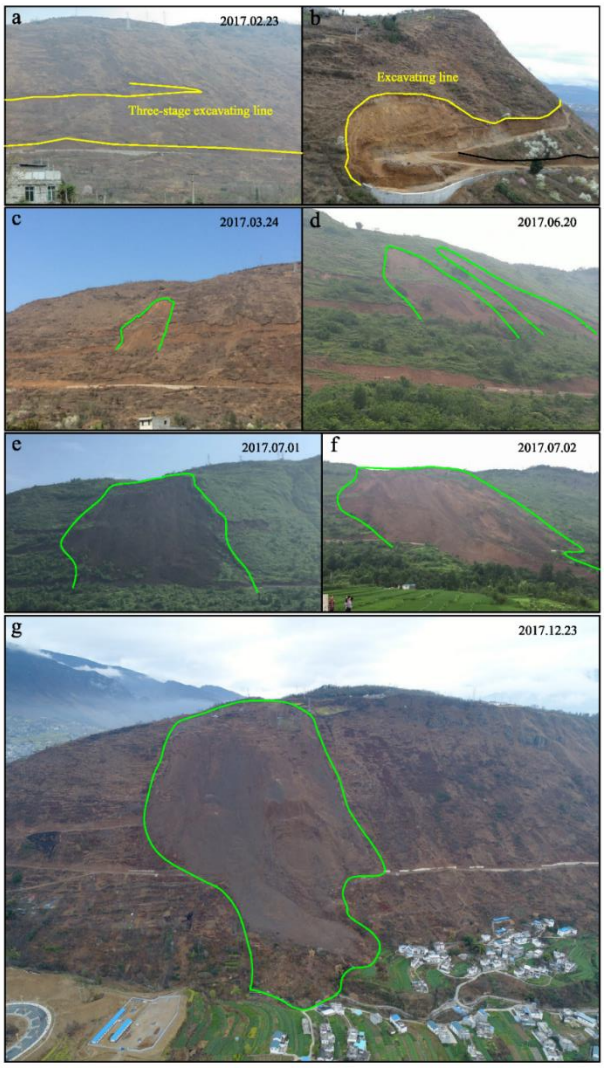

Fig. 2 Recorded processes of the Lantian landslide. (a) and (b). Three stages beltway excavating on the slope, (c). Local collapse occurred on 24, March, (d). A new local sliding occurred on 20, June, (e). Large-scale sliding on 1, July, (f). Overall sliding occurred on 2, July and (g). The sliding mass tended to be equilibrium

Xiaojiang fault zone and the southeast boundary of Mile-Shizong fault zone. Due to the intensive tectonic activities, the study area had experienced frequent earthquakes, the development of active faults, and multiple stages magma activities. The landslide area is sandwiched between Majiahe dam thrust fault and Leibo fault, both of which have the strike of North-East (Fig. 1(b)). The Leibo fault zone consists of three nearly parallel Northeast-Eastward secondary faults. The faults composition, from north to south, is the north branch fault (F1-1), the middle branch fault (F1-2), and the south branch fault (F1-3), which constitute a total length of 35 km and width of 10 km NEE fault zone (Han *et al.* 2009). The Majiahe dam fault here strikes NE with 17 km in length and 5 km in width, can be split into front thrust compression zone, middle subduction shear zone, east oblique reverse fault-strike-slip shear zone, west normal fault strike-slip zone and rear tectonic deformation zone, with curves as "W" shape in the plane and "S" shape in the profile (Liu *et al.* 2006). The secondary faults in the study area well develop, resulting in regional lithological fragmentation. In addition, the NNW-trending Ebian-Jinyang fault, the NE-trending Lianfeng fold zone and the Northeast Mabian-Daguan seismic fault zone constitute a nearly three-sided closed tectonic plate, called the Leibo-Yongshan triangle block, during which the stress is concentrated and locked. Earthquakes are easy to concentrate due to the unbalanced local strain of the tectonic stress field (Fig. 1(b)).

Lithologically, the bedrock belongs to Permian Emeishan basalt formation ($P_2\beta$), which primary is intermittent fractured multi-centered basalt with an average thickness of over 400 m (Lin 1985). Basalt often represents by the characteristics of hard, relatively complete, strong weathering resistance and high strength. However, in the landslide area, owing to multiple factors involving tectonic movement, weathered unloading, mass wasting, the basalt is completely-highly weathered, with a depth over 30 m. As aforementioned, the Lantian landslide was the resurgence of an ancient landslide. The sliding surface of the ancient landslide was the interface between highly weathered basalt

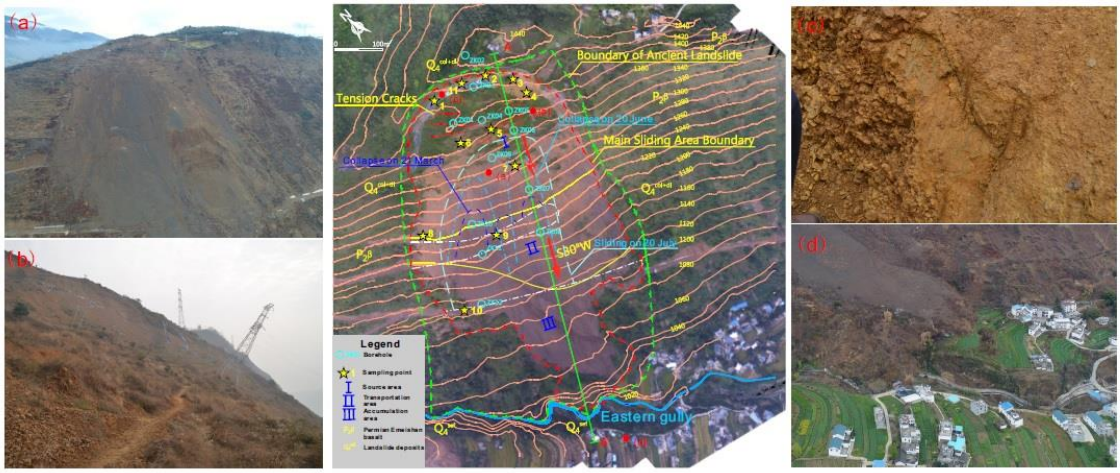

Fig. 3 Geological and topographic map of landslide area and the distribution of in situ investigation points. The base map is a digital orthophoto from 23 September 2017. The topographic contours have been simplified. The sliding mass samples were collected from points 1 to 10. The slipping zone soil samples were collected from boreholes ZK01, ZK04; ZK05, ZK06, ZK07, ZK09. The bedrock samples were collected from points 11 in the detachment scar and boreholes ZK01~ZK12. (a) Aerial view of the headscarp of landslide, (b) Oblique electrical tower, (c) The outcrop sliding surface descended from the fresh scarp on the upper slope and (d) Buildings near the Lantian landslide

and moderately weathered basalt. The Quaternary stratum includes a deluvium, eluvium and landslide deposits layers. The Quaternary deposits dominantly consist of soil and rock debris that originated from the basalt rock.

This area belongs to a subtropical monsoon climate with a mean annual temperature of 14.7℃. The average annual rainfall in Lantian landslide area is about 586.3~851.2 mm, and 90.37~96.55% of it is concentrated from June to September with many rainstorms.

3. Features of Lantian landslide

3.1 Occurrence of the Lantian landslide

Excavation of the beltway began on August 16, 2016. Three platforms were excavated successively without any retaining measures (Figs. 2(a) and 2(b)). Attributed by the excavation on the ancient landslide deposits, the rock and soil mass within the slope experienced unloading and relaxation deformation, leading to a shallow collapse on the upper part of platform on March 24, 2017. The local collapse had a length of about 110 m and a width of about 90 m, comprising of fully-highly weathered and fractured basalt (Fig. 2(c)). Since June, 2017, the study area entered the rainy season. On June 20, 2017, the collapse area did not expand, however, a new collapse occurred on the left side of the former one (Fig. 2(d)). On July 1, affected by continuous antecedent precipitation, the slope showed an accelerated sliding, and the previous collapse expanded (Fig. 2(e)). The rear edge reached the platform at the upper part of slope and an electrical tower at the platform did not fall, indicating the incomplete reactivation of the ancient landslide. On July 2, due to the retrogressive failure of the slope, the overall sliding occurred and formed debris flow downslope (Figs. 2(f) and (g)).

3.2 Geometry

Fig. 3 shows the location of the landslide. The landslide extends westward from a crest bench and downslope to the toe area on the left flank of the Eastern gully at an altitude of 1020 to 1420 m. It has a length of 510 ~ 741 m, a width of 350 ~ 410 m, and a maximum depth of 76 m, a ground surface area affected by the landslide of approximately 22×10^4 m^2, a reactivation volume of 403×10^4 m^3, with 75 % sliding mass stranded in the source area, and a sliding direction of SW30º. The post-landslide gradients are diverse in different parts, for 50 ~ 60º in the upper part, 33º in the middle part, 20º in the lower part, respectively (Fig. 4).

The landslide thickness was extracted from 12 drilling boreholes. Fig. 5 shows the vertical distribution of rocks and soils of the Lantian landslide. The sliding zone was found at the depth of 27.64 ~ 76.40 m from the ground surface in the source area, with a thickness of 0.30 ~ 2.20 m. By investigating the topography of slope on the surrounding area, the original terrain of the source area was restored. Combined with the drilling data, we determined the general shape of the sliding zone, which can be divided into three sections: the steep section at the rear edge, the sliding section in the middle and the gentle section at the front (Fig. 4). The soils involved in the slip zone were characterized by gray, grayish-yellow, grayish-green with breccia debris, clay, and breccia clay, with a grain size distribution of 0.2 ~2 cm. It is noteworthy to say that a clear scratch can be discovered in the borehole profiles, which can be asserted as the evidence for the landslide movement (Fig. 5(b)). The drilling profile is shown in Fig. 5(a).

3.3 Zones of the Lantian landslide

The landslide involves three zones (Fig. 3): the source area (Zone I), the transportation area (Zone II) and the

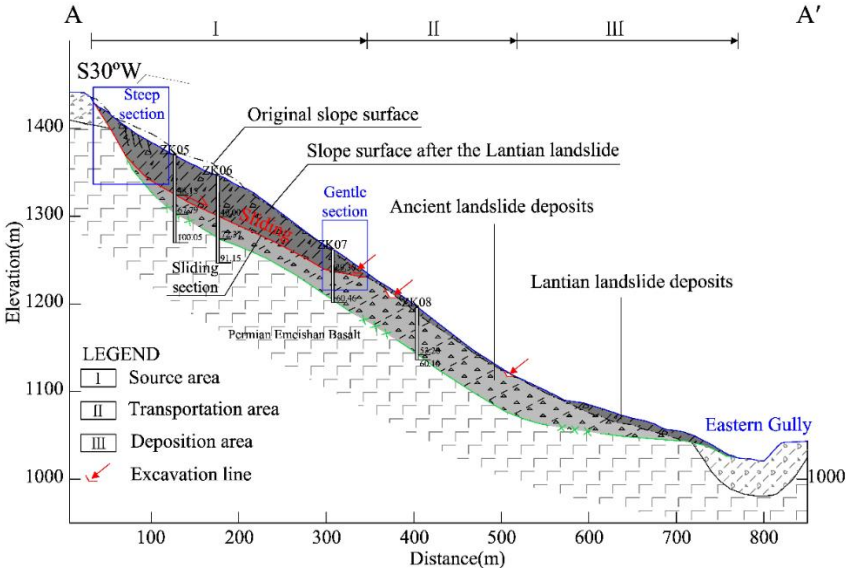

Fig. 4 Geological profile of the Lantian landslide (section A-A' in Fig. 3)

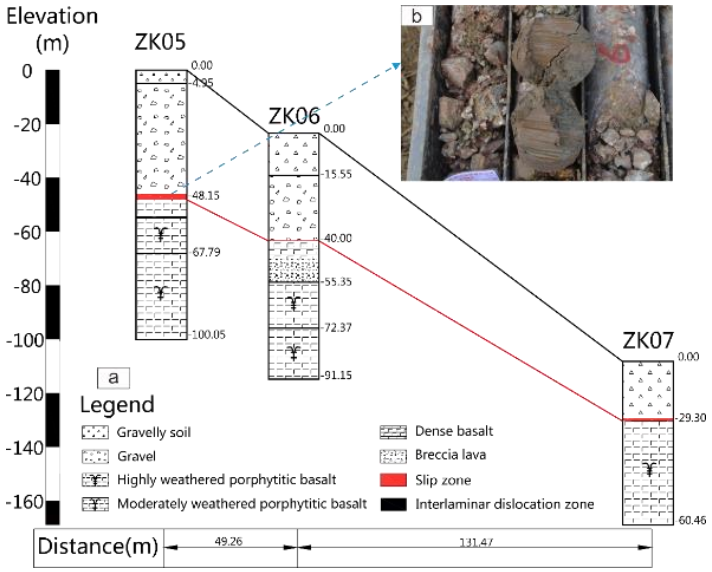

Fig. 5 Simplified stratigraphies of some boreholes, located as shown in Fig. 3

deposition area (Zone III). This section described the characteristics of each zone.

3.3.1 Source area (Zone I)

The landslide was initiated from the upside of the slope, with the elevation ranging from 1200 to 1380 m, a height difference of about 180 m, and a sliding direction of SW30°. The source area has a length of 300 m, a width of 360 m, a slope of 15°-60°, an area of 9.6×10^4 m^2. The average deposition thickness of this area was about 45 m, leading to a volume of 303×10^4 m^3. Based on the investigated results, the fully to strongly weathered basalts in this area mainly maintained the original structure after sliding, about 75% of the total volume. About 25% volume of the basalts slid from the shear outlet and formed debris flow in the further movement. In addition, the electrical tower showed an oblique deformation without severe topple down (Fig. 3(b)). Thus, the moving pattern of the source area was mainly an overall sliding with relatively slow velocity, and after sliding, this zone formed a banded main scarp in the rear edge, with a height of 10-17 m, a slope of 50°-60°. From the basalt rock mass structure observed in the main scarp, the joints and fissures were well developed in the landslide area, with weathered clay filling in the interval (Fig. 6). This fractured structure was favorable to slope failure and disintegration under the role of external disturbance.

3.3.2 Transportation area (Zone II)

The transportation area is 50-190 m long in the sliding direction and 430 m wide in the middle part of the slope, with the elevation varying from 1200 to 1270 m, the slope of 35°-40°, the sliding direction of SW30°, and an area of 5.5×10^4 m^2. The deposition thickness is about 2-7 m, leading to an volume of 30×10^4 m^3. The sliding mass in this

Fig. 6 Characteristic of the source area. (a) Gentle platform formed in the rear edge of source area due to the slow sliding velocity, (b) Banded main scarp in the source area, (c) Fractured rock masses observed in the back wall and (d) Residual landslide monadnock deposited in the source area

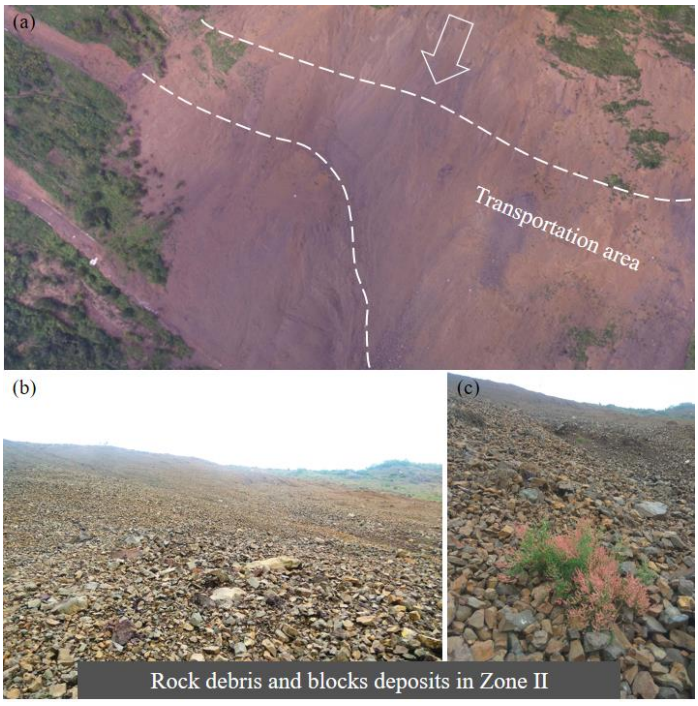

Fig. 7 Characteristic of the transportation area. (a) General geomorphology of this area, (b) and (c) small size rock debris and blocks deposits

zone was completely disintegrated and transformed into rock debris and blocks, with the size of 5-53 mm.

3.3.3 Deposition area (Zone III)

At the elevation of 1270 m, the gradient of slope turns to gentle, which led to the rock debris and blocks depositing in this zone. The deposition area has a slope of 15°-20°, an area of 7×10^4 m^2, an average thickness of 20 m, and a volume of 14×10^4 m^3. The deposits reached the Eastern gully at the toe and dammed the gully (Fig. 8). Different from the deposition characteristics of the Zone I and Zone II, the rock blocks with large size in the deposition area were much more, probably owing to the slow moving velocities in this zone.

Fig. 8 Characteristic of the deposition area. (a) Gentle slope at the toe of slope, (b) General geomorphology of this area, (c) The Lantian landslide dammed the Eastern gully at the toe and (d) Large size rock blocks in this area

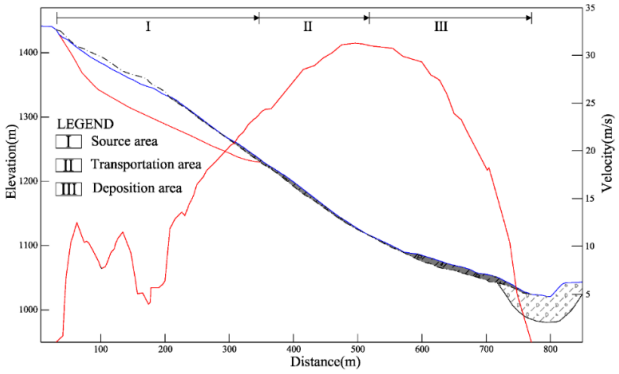

Fig. 9 Velocity distribution of the landslide

3.4 Material composition

A site investigation involving the laboratory tests and boreholes was performed after the catastrophic event of July 2017. In order to obtain the stratigraphy of the landslide, twelve boreholes were drilled. The failure mass was mainly composed of basaltic blocks filled with clay, about 50 m in thickness at the upper part and 30-40 m at the middle-lower part of the landslide. A 0.30 ~ 2.20 m thick slip zone composed of breccia debris, clay, and breccia clay was identified within the old landslide deposits. The bedrock was composed of moderately weathered basalt.

Several soil and rock samples were collected from in-place bedrock outcrops, loose landslide debris, detachment scar, and drill cores for accurate physical and mechanical parameters assessments (Fig. 3). The results from the laboratory tests indicated that the grain size distribution of soils of sliding zone varies from silt with gravel to fine-grained gravel, with clasts of less than 5 mm accounting for 33.0% ~ 70.0%, less than 0.075 mm accounting for 8.5% ~ 30.9%, less than 0.005 mm accounting for 3.8% ~ 7.5%, respectively. In terms of the deposits soils, which varies from clay with gravel to silt with gravel, with particle content of less than 5 mm accounting for 55.1% ~ 59.0%, less than 0.075 mm accounting for 19.8% ~ 27.6%, less than 0.005 mm accounting for 7.2% ~ 10.0%, respectively.

3.5 Dynamic characteristics of the landslide

Scheidegger method was often adopted to estimate the velocity of the landslide-debris flow (Scheidegger 1973).

We measured the maximum vertical travel distance of 250 m, the maximum horizontal travel distance of 520 m. The equation was following

$$V=\sqrt{2g\left(H-f\bullet L\right)} \quad (1)$$

While V is the moving velocity, *m/s*, g is the gravity acceleration, m/s^2; H is the height difference between the crown of the source area and the calculation point, *m*; f is the apparent coefficient of friction, which is the ratio of total height difference to the travel distance, equaling to 0.557 (412/740); L is the horizontal distance from the crown of the source area to the calculation point, *m*. The cross-section A-A' was utilized to calculate the velocity changing during the landslide rouout.

Fig. 9 shows the calculation result, suggesting that there is an obviously increasing and decelerating of the velocity from the initiation to deposition, with a maximum value of 31 m/s. After the rock debris slid to the front gentle slope, especially below the elevation of m, the velocity decreased dramatically. According to the velocity classification of landslide, the Lantian landslide would be described as a very rapid landslide with short runout distance.

Table 1 Physical and mechanical parameters of strata

Condition	lithology	Unit weight(kN/m^3)	Elastic modulus (MPa)	Poisson's ratio	Cohesion (kPa)	Friction angle (°)	Ks (m/s)	Θs(%)
Natural condition	Sliding mass	23.5	45	0.33	18.5	25.3	3.45×10^{-5}	23
	Moderately basalt	28	30000	0.27	600	38	/	/
	Colluvial deposits	25.5	50	0.30	30	28	1.27×10^{-5}	18
	Alluvial deposits	26.5	55	0.29	35	30	8.3×10^{-6}	15
Rainstorm condition	Sliding mass	24.5	40.3	0.32	16.8	23	/	/
	Moderately basalt	28.5	28000	0.25	590	37.5	/	/
	Colluvial deposits	26.0	48	0.29	28	26	/	/
	Alluvial deposits	27.0	52	0.27	32	29.5	/	/

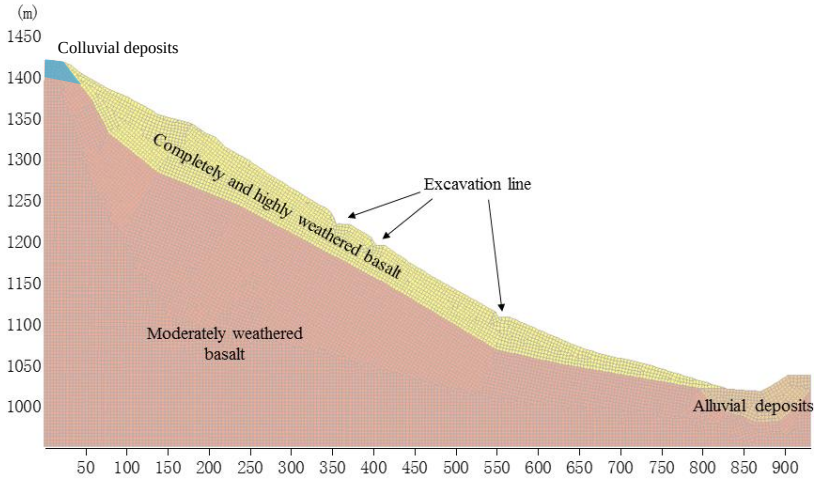

Fig. 10 The calculation model of profile A-A' in Fig. 3

4. Numerical modelling of the landslide

Based on the occurrence of Lantian landslide, road excavation and precipitation prime the slope for failure. To further and quantitatively clarify the deformation and failure mechanisms of the Lantian landslide subjecting to excavation and rainfall, numerical modellings were carried out to explore the displacement, strain and seepage field of the slope.

4.1 Calculation model

The Geo-Studio software (Geo-slope Ltd. 2007a, b) for ascertaining groundwater variation and stress distribution problems in deposit materials was performed to analyze the landslide. The main geological profile A-A' was employed for the calculation model (Fig. 10). The materials contained 4 kinds of material. Based on direct shear test in laboratory, the mechanical and physical parameters of materials were obtained. The saturated permeability coefficient (Ks) and saturated water content (Θs) were obtained by water injection test in the boreholes. These parameters were listed in Table 1. The hydraulic behavior of the rock-soil mixtures was estimated by the van Genuchten model (Genuchten 1980). The elastic-plastic constitutive model was performed for the calculation model and all the material was based on the Mohr-Coulomb yield criterion. The model was 843.3 m in length, 491.5 m in height on the left boundary and 93.5 m in height on the right boundary. For the seepage analysis, the bottom and right side boundaries were assigned as a drained boundary. The left boundary was the fixed head boundary, its height was 1420 m. Rainfall data from 19 June to 2 July was applied as boundary condition at the slope surface (Fig. 11). The groundwater table was obtained by drilling boreholes. For the finite element model, the left and right boundaries were set as no-horizontal displacement boundaries, and the bottom boundary was set as a fixed boundary in both horizontal and vertical direction. The calculation process was based on the actual occurrence sequence of the slope, which was divided into three steps: First, the original slope status before excavation was simulated. Second, the excavation condition is simulated

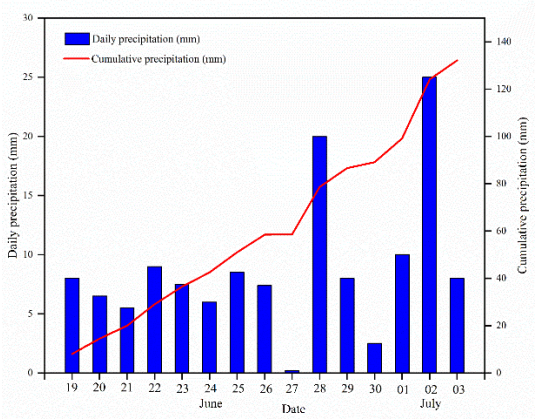

Fig. 11 Daily and cumulative precipitation from 19 June to 3 July

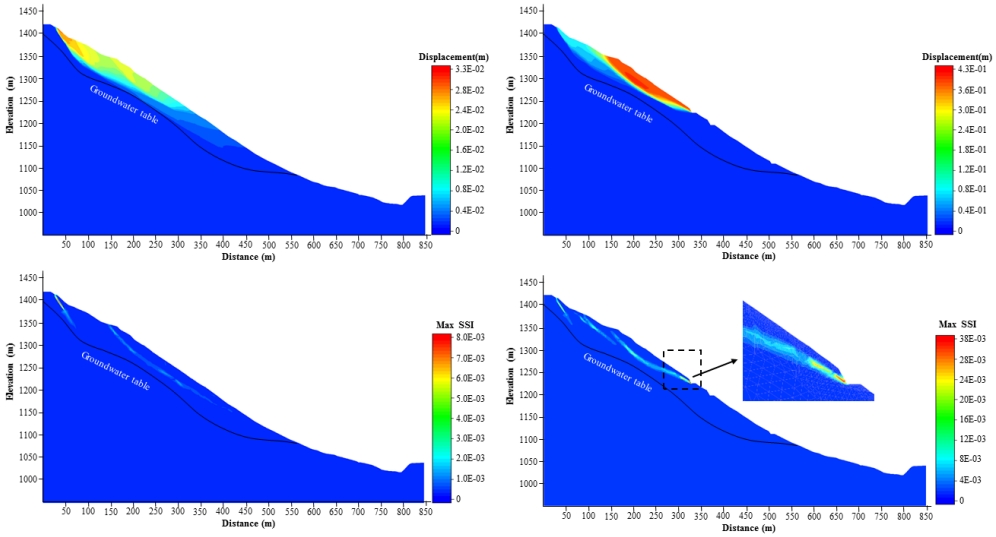

Fig. 12 Total displacement of the slope before (a) and after (b) excavation; Maximum shear strain increments of the slope before (c) and after (d) excavation

while three platforms were excavated. The third step was to simulate the rainwater infiltration condition of the slope after local collapse.

4.2 Excavation

The excavation process is simulated as three-stage excavation. Fig. 12 shows the maximum shear strain increment (Max SSI) and displacement of the slope before and after excavation. It is suggested that the original slope is in stable state (Figs. 12(a) and 12(c)). With the excavation, Sub-vertical free surface formed in the slope, and the strain at the toe and the slope is redistributed progressively. The Max SSI at the toe is about 3.8×10^{-2}, and is clearly concentrated at the excavated free surface (Fig. 12(d)). The Max SSI at the shear outlet was relatively significant, and it decreased from ground surface to the inside of the slope. A small shear strain concentration zone can be observed at the rear edge of the slope. The rock-soil mixture near the upper free surface appears unloading deformation. And the maximum total displacement reaches 43 cm (Fig. 12(b)), which is in agreement with the shallow local collapse of the slope on March 24, 2017 (Fig. 2(c)).

4.3 Rainfall

After the local collapse of the slope, the road construction was terminated. The slope entered a slow creep deformation stage. Because of the intense rainfall on 2 July and prolonged antecedent rainfall, water infiltrated into the slope. Water ponds at the upper slope appeared, the water content of the slope increased and the geomaterials of the slope became softened. The upper part of the slope is saturated over a long period of antecedent rainfall. The rainwater concentrated the slope to raise the groundwater level in the slope and caused the pore water pressure to increase, thus induced an entire sliding event (Figs. 13(c) and 13(d)). It can be observed that closed isolines were formed inside the upper part of the slope during infiltration and that the pore water pressure isolines near the ground surface were wider, indicating that the infiltration progressively diffused into the interior of the slope. Fig.

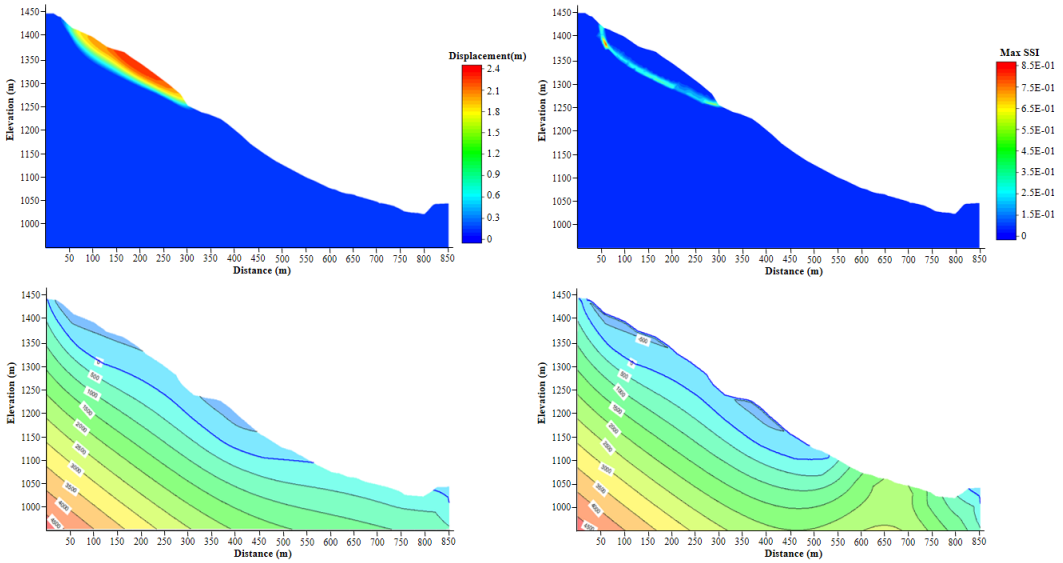

Fig. 13 (a) Total displacement of the slope due to rainfall, (b) Maximum shear strain of the slope due to rainfall; Pore water pressure distribution of the slope before (c) and after (d) 14 days rainfall

13(a) shows the total displacement contour map of the slope after prolonged precipitation. The maximum total displacement simulated is 2.4 m, which is located at the upper slope, which is consistent with the large-scale deep-seated landslide on July 2, 2017 (Fig. 2(f)). Under the influence of incessant rainfall, a large Max SSI appears within the slope, with a value of 8.5×10^{-1} (Fig. 13(b)). Different from the contribution of excavation, the maximum SSI showed a concentration effect on the potential sliding zone, which probably induced the connection of the sliding zone.

According to the above analysis, road excavation on the slope led to stress concentration at the engineering position, and declined the slope stability, and then local collapse occurred. Antecedent and intensely instantaneous rainfall resulted in increasing groundwater and pore water pressure, as well as softened the rock-soil mixtures. The retrogressive slide occurred at the upper section of the slope, due to the high locality and the unconsolidated geomaterials, the landslide-debris flow formed that produced a severe hazard.

5. Causative factors attributed to the landslide

5.1 Predisposing factors

The onset of landslides can be influenced by predisposing factors involving local topographic factor and geologic factor (Liu *et al*. 2020). The latter includes geological structures, stratigraphy, and the tectonic movements (Zhang *et al*. 2020).

5.1.1 Topographic influence

The high and steep terrain conditions the initiation and runout of landslide. The landslide area, located at a middle mountain region, has a height difference of 400 m. This character was beneficial to accumulate strain energy. The source area has the high-locality effect which can promote high-speed moving of the landslide. The topography in the middle part of the slope was relatively steep, with a gradient of 35°-40°. The steep slope provided a favorable free surface for the disintegration and acceleration of the Lantian landslide. When the landslide slid from the source area, the sliding mass experienced collision, scratch and disintegration when passing the middle part of the slope, and the moving pattern varied from overall sliding to debris slide. On the one hand, the steep slope of this region had a certain accelerated effect for the landslide, as well as increased the volume of the landslide. On the other hand, the large area of this region limited the movement of the rock debris and reduced its kinetic energy. Therefore, the moving pattern in this region mainly involved weak scratch with thin accumulation. The front of the slope has a gentle gradient of 15°-20°, which resulted in relatively low velocity in this region. Then, the Eastern gully at the toe induced deposition of the rock debris due to the resistance of the deep gully. Consequently, the different topographic conditions of the slope determined the initiation and migration form of the landslide.

5.1.1 Geologic influence

The geologic factor mainly had a degradative influence on the rock mass in the landslide area. The location of the landslide near the tectonic active zone and its geological features of fractured rocks indicate that the landslide occurrence is dramatically influenced by active tectonic roles. The Lantian landslide is located in the three-sided closed tectonic block called the Leibo-Yongshan Triangle, which is surrounded by the northwestern Zemuhe fault in the west, the northeastern Lianfeng fault in the southeast, and the northwestern Mabian-Daguan fault in the northeast. The closed block, in which the stress is concentrated and locked, the seismic activity is frequent due to the local strain imbalance of the tectonic stress field. Moreover, the

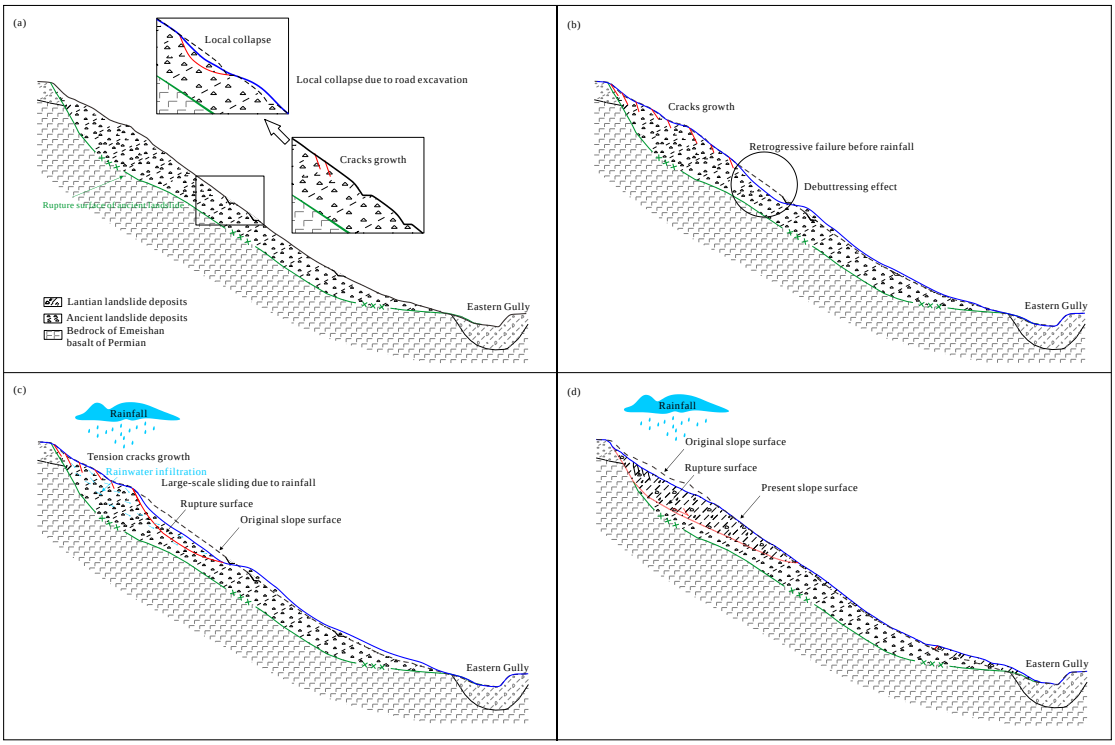

Fig. 14 Formation mechanism of the Lantian landslide. (a) Local collapse at the upper slope due to the road excavation, (b) Shallow landslide under the role of gravity, (c)-(d) Occurrence of large-scale landslide caused by intense rainfall

Lantian landslide is located in the hanging wall of the Maijiahe dam fault, which can further reduce the integrity of rock masses.

Tectonic movements in this region mainly include folding movement in the Himalayan orogenic period. The extension and compression of multi-stage folding to the brittle basalt rock mass leaded to the formation of massive structural planes. Furthermore, in the context of long-term weathering, retiform shape fissures were well developed throughout the basaltic rock mass, and clay content increased significantly, forming the "soil mixed with rock" structure. The fractured and highly-weathered basalt materials provide a favorable condition for the water to permeate the rock mass deeply to form a high groundwater table. The heterogeneous and unconsolidated slope materials are easily sliding when experienced external disturbance. After the rock mass slid, due to the release of stress, the friction between the sliding mass and the ground, and the mutual shear and collision within the sliding mass, the rock masses would dislocate along the discontinuities, resulting in the destruction of rock mass structure and the formation of debris flow.

5.2 Triggering factors

5.2.1 Road excavation

The improper design of slope excavation and stabilization is considered as a contributing factor to the Lantian landslide. Excavation without proper support helps trigger the landslide through exposing geological structures on the free surface and by unloading the toe of the slope (Stark *et al.* 2005). The multi-excavation with high and steep cut slopes can be observed along the beltway. Field investigation prior to excavation presents that the original slope was stable. Three stage excavating of the beltway was conducted, with an excavating height of 10-15 m, and a volume of 1.5×10^4 m^3. On the one hand, the local and entire failure indicates that the excavation has a direct impact on the stability of slope by unloading of the cut slope and redistributing of the stress. Additionally, road intercepted subsurface flow from cut slope during storms and concentrated overland flow on their paved surfaces. Therefore, the resistance sliding force of slope was reduced, gravity-induced slope failures occurred on the cut slope. On the other hand, the sliding zone has a geometry of steep back edge and gentle front edge. Before the excavation, the landslide body reached a relatively equilibrium stage, and the gentle shear outlet at the front edge formed an anti-sliding section. Because of the excavation, small-scale local collapse occurred in the middle of the slope. Thus, the anti-sliding section was disturbed, and the sliding resistance force decreased, providing a favorable condition for the overall slippage of the slope.

5.2.2 Rainfall

Fig. 11 shows the rainfall data before and after the landslide occurrence. Instantaneous high-intensity rainfall was the main triggering factor for the Lantian landslide. Daily rainfall reaches 10 mm on 1 July and 25 mm on 2 July, and a cumulative rainfall is 124.1 mm from 19 June to 2 July. Since the ancient landslide body has high permeability, water not only resulted in shallow soil saturation but also infiltrated deeply into the rock mass, thus increasing the probability of slope failure. The weathering

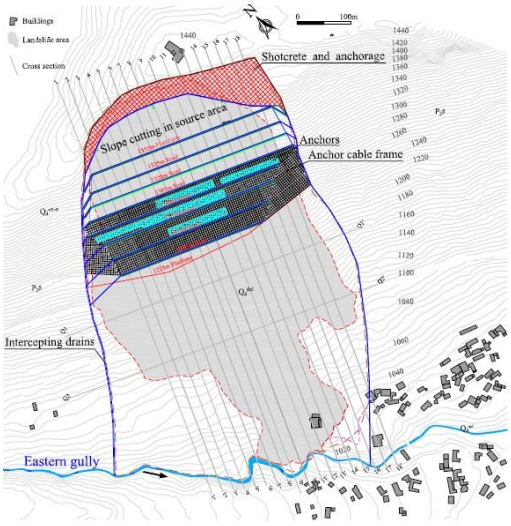

Fig. 15 Overview of technical solution to the failed slope

with the groundwater has a significant effect on producing fatigue and damage in sliding mass when landslides are distributed in active tectonic regions. Before heavy rainfall in the landslide area, the deformation was still ongoing but in a slow speed. The rainfall accelerated the resurgence of the ancient landslide markedly. Therefore, rainfall presented a major triggering factor for the reactivation of the Lantian ancient landslide.

6. Formation mechanisms of landslide

Based on the results of geological survey and numerical modelling analysis, the formation conceptual model of the Lantian landslide is posed (Fig. 14). The model involves two continuous sliding stages, which are described in detail in the following sections:

Stage 1 Initiation of landslide caused by excavation

The beltway excavation work performed increased the steepness and height of the slope. As described above, the sliding zone mainly consists of three sections: the rear edge steep section, the middle sliding section and the front gentle section. Thereinto, the latter two sections are considered as the anti-sliding section of the landslide. The influence of the excavation work on the slope caused a redistribution of the stress and concentration at the toe of the cutting slope, thus increased the slope deformation locally. When the slope deformation reached a limit state, tensile cracks would appeared in the ground surface. Finally, the fully-highly weathered fractured basalt rock mass collapsed along the free direction (Fig. 14(a)). After that, new free surfaces produced, leading to the shallow sliding of the upper part of slope and the occurrence of more tension cracks. Under the role of gravity, the slope continued to sliding with a nature of retrogressive moving until the failure reached the gentle platform at the rear edge (Fig. 14(b)). Site evidence that the electronic transmission tower at the rear of slope did not fall during this stage showed mass movement was not completely sliding of the slope.

Stage 2 Overall failure of the landslide and transforming into debris flow

The cracks in the slope were filled up by infiltration water because of the rainfall during 19 June to 2 July, which caused the cracks propagating, pore water pressure growing, and shear strength reducing of the slope, then cohesion loses and effective friction angle on sliding zone decreased saliently on wetting state, resulting in overall sliding (Figs. 14(c) and 14(d)). During this process, due to the different dip angle of the sliding zone, combined with the friction within the sliding mass, the speed of each section of the sliding mass is inconsistent. The speed of the rear edge is rapid that it of the front edge, forming landslide benches and scarps in the slope. The rock masses detached from the source area collided, compressed and rubs with the original ground surface, disintegrated rapidly along the structural planes in the rock mass and transformed into the debris flow rolling down the slope, and finally accumulated at the gentle front of the slope.

7. Proposals for countermeasures

Since some buildings have been built on the gentle slope at the toe of the slope, and the new district of the county is planned. Because of the large thickness and complex structure of the landslide, the strong deformation of the reactivation area, the large distribution of cracks at the back, and the serious damage of the soil structure, if the full excavation scheme is adopted, not only the work amount and cost are huge, but also the high and steep slope formed after excavation will generate new stability problems. If anchor cable or anti-slide pile is directly used for treatment, the length and size of the anchor cable or anti-slide pile are too large due to the large thickness of the sliding mass, which is difficult and infeasible in the technology and construction.

Based on the analysis on the causative factors and failure mechanism, a comprehensive slope stability solution

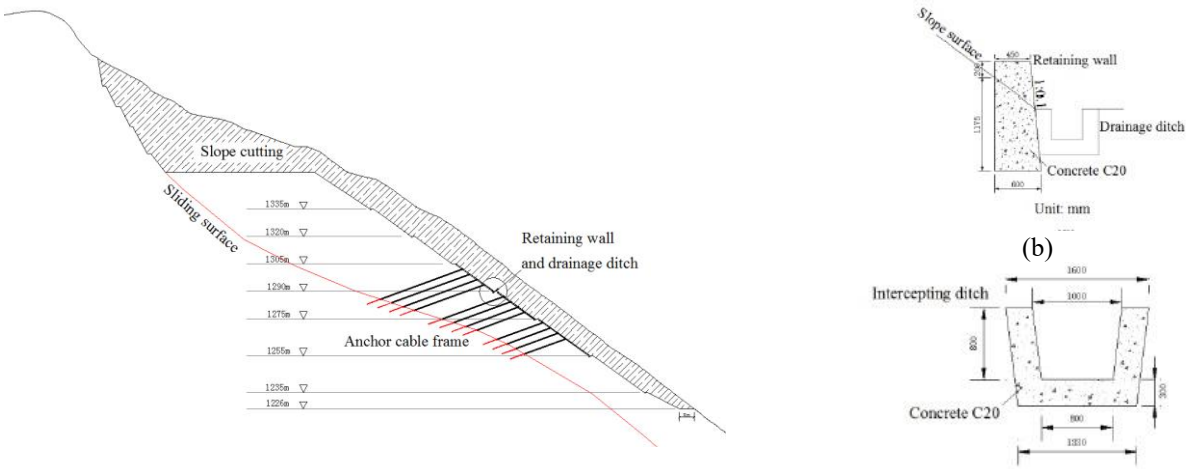

(a) (b) (c)

Fig. 16 (a) The design of the mitigation measure on the profile 10-10', (b) The design details of the retaining wall and (c) the intercepting ditch

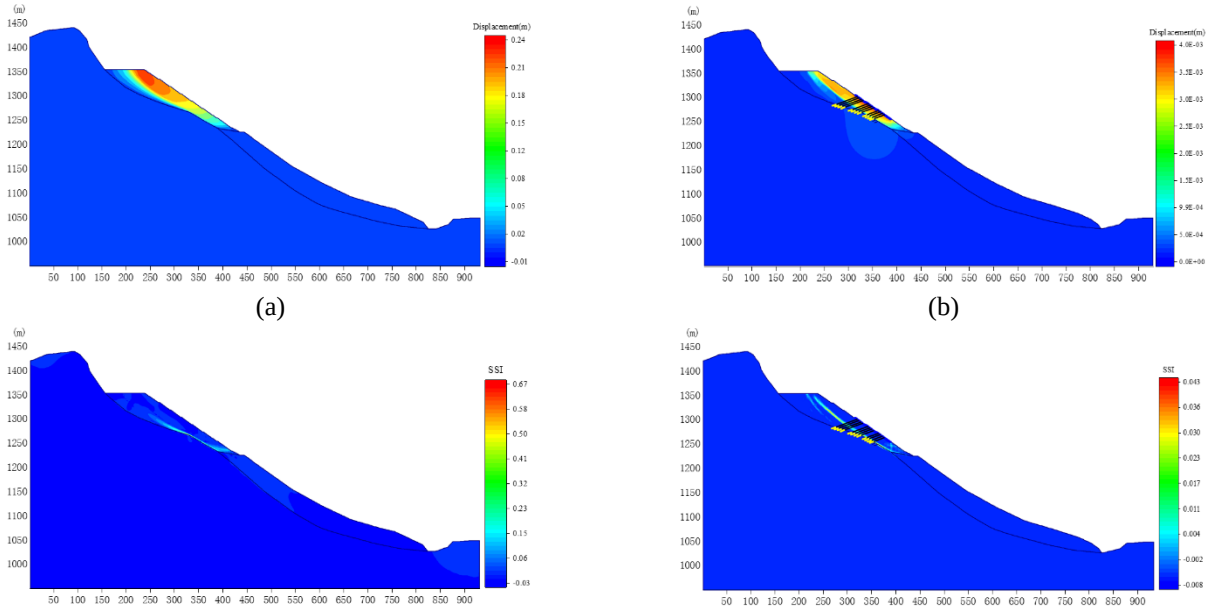

(a) (b) (c) (d)

Fig. 17 Total displacement of the slope before (a) and after (b) excavation; Maximum shear strain increments of the slope before (c) and after (d) excavation

was posed to stabilize the failed slope and prevent future landslides, including slope cutting, anchor cable frame, anti-sliding retaining wall, and intercepting ditch (Fig. 15). The failed slope was cut to form a new geometry, including a total of 9 blocks (from shear outlet to the top of the slope), with each block having a height of 15-20 m. The ground anchors and reinforced concrete frame were set up at the 3rd to 5th blocks, with retaining wall employed at the toe of each block (Fig. 16(a)). The retaining wall is 1.4 m high, with a width of 0.45 m at the crest (Fig. 16(b)). The intercepting ditch was set up at the lateral margins of the landslide, with a bottom width of 0.8 m, a depth of 0.8 m, a length of 950 m, a furrow bank that is 0.3 m wide, and a ditch base that is 0.3 m wide (Fig. 16(b)). The total number of anchor cables is 350, the anchorage length is 10 m, and

Table 2 The anchor properties

Name	Unit	Anchor
Axial stiffness (EA)	kN/m	2.0E7 (anchorage-segment) 2.0E5 (Free-segment)
Pre-stressed force (Nc)	kN/m	500
Length	m	30-60
Diameter	m	1.5
Spacing	m	4
Angle from horizontal	degree	20
Number of tendons per anchor		7

Table 3 The material properties of concrete frame

Name	Unit	Concrete frame
Axial stiffness (EA)	kN/m	1.1E7
Flexural stiffness (EI)	kN/m	5000
Equivalent thickness	m	0.074
Unit weight	kN/m^3	0
Poisson's ratio		0.2

the length of free-segment is 20-50 m. The center distance between the two adjacent anchor cables is 4.0 m. Fig. 15 shows the plane view of the designed mitigation measures.

The slope stability analysis was conducted on the Plaxis 2D model to examine the appropriate solution (Brinkgreve *et al.* 2010, Fawaz *et al.* 2014). Profile 10-10' in Fig. 15 was selected as the calculation model. The total displacement and SSI on the designed slope after employing the countermeasures are presented in Fig. 17. The stability factor related to the existing sliding surface (both ancient landslide and reactivated landslide sliding surfaces) was also calculated using strength reduction method, with a magnitude of 1.442 and 1.628, respectively. The Lantian landslide with engineering control measures would become stable under rainfall or earthquake conditions.

8. Limitation

Based on the mechanics data and detailed geological investigations of landslides, the deterministic analyses of landslides for investigating the corresponding failure mechanisms have been proved in previous studies (Ma *et al*. 2018, Wang *et al*. 2021, He *et al*. 2021b, Liu *et al*. 2021). Although the inherent heterogeneity of geomaterials (e.g., cohesion and friction angle) may influence failure behaviour or stability of geo-systems (Nguyen *et al*. 2017, 2019, Ma *et al*. 2021b, c), the deterministic analysis has been widely demonstrated as a reliable approach to investigate failure behaviour and its mechanisms. However, if the spatial variability of soil shear strength could be considered in this work as a compensation for current analysis, the computational results could be more comprehensive compared with the conventional approach. Hence, the probabilistic slope stability analysis should be considered in future works.

9. Conclusions

In this paper, the characteristics, causative factors, failure mechanisms of the Lantian reactivated landslide in Leibo County were investigated by field investigation and numerical modeling. Several conclusions can be drawn from this study:

1. The landslide occurred in the active tectonic region of Leibo-Yongshan Triangle. Due to the historical tectonic movement, the geological structure was characterized by completely and highly weathered basalt that is favorable for rainwater infiltration, consequently resulting in the rising of groundwater table in deep layers of the slope. Thereby these conditions were benefit to landslides.
2. The numerical analysis indicated that except for the predisposing causes of the landslide, the road excavation factor was a predominant contributing factor. Moreover, rainfall occurred from 19 June to 2 July with 14-days accumulation of 124.1 mm generated high pore water pressure, and raised the groundwater level, finally triggered the large-scale landslide.
3. A comprehensive mitigation measures were designed and conducted to stabilize the failed mass and prevent potential landslide risk in future. Compound solutions including anchor cables, retaining wall, and intercepting ditch have been utilized to this case study. The findings not only provide a good case study on coupled excavation and rainfall-induced landslides but are also a useful reference in solving practical problems regarding slope remedy along roads in China.

Acknowledgments

The research described in this paper was financially supported by the National Key Research and Development Program of China (2018YFC1505401), the National Natural Science Foundation of China (41731285), and the Youth Fund Project of NSFC (41907225) and Open fund of State Key Laboratory of geological disaster prevention and geological environment protection (Grants No. SKLGP2018K011), and the China Scholarship Council (202107000060).

References

Abderahman, N. (2006), "Evaluating the influence of rate of undercutting on the stability of slopes", *Bull. Eng. Geol. Environ.*, **66**(3), 303–309. https://doi.org/10.1007/s10064-006-0078-6.

Acharya, K.P., Yatabe, R., Bhandary, N.P. and Dahal, R.K. (2014), "Deterministic slope failure hazard assessment in a model catchment and its replication in neighborhood terrain", *Geomat. Nat. Haz. Risk*, **7**(1), 156-185. https://doi.org/10.1080/19475705.2014.880856.

Acharya, K.P., Bhandary, N.P., Daha, R.K. and Yatabe, R. (2015), "Numerical analysis on influence of principal parameters of topography on hillslope instability in a small catchment", *Environ. Earth Sci*., **73**, 5643-5656. https://doi.org/10.1007/s12665-014-3819-z.

Ali, J.R., Thompson, G.M., Zhou, M.F. and Song, X. (2005), "Emeishan large igneous province", SW China. *Lithos*, **79**(3-4), 475-489. https://doi.org/10.1016/j.lithos.2004.09.013.

Boulfoul, K., Hammoud, F. and Abbeche, K. (2020), "Numerical study on the optimal position of a pile for stabilization purpose of a slope", *Geomech. Eng*., **21**(5), 401-411. https://doi.org/10.12989/gae.2020.21.5.401.

Brinkgreve, R.B.J., Swolfs, V.M. and Engin, E. (2010), Plaxis 2D 2010. Manual.

Cheng, X.F., Zhu, C.B., Qi, W.F., Xu, J. and Yuan, J. (2015), "Formation conditions,development tendency and preventive measures of pufu landslide in luquan of Yunnan", *Mineral Resources & Geology*, **29**(3), 395-401. (In Chinese)

Crosta, G.B. (2003), "Distributed modelling of shallow landslides

triggered by intense rainfall", *Nat. Hazard. Earth Syst. Sci*., **3**, 81-93.

Fawaz, A., Farah, E. and Hagechehade, F. (2014), "Slope stability analysis using numerical modelling", *Am. J. Civ. Eng*., **2**(3), 60-67. https://doi.org/10.11648/j.ajce.20140203.11.

Froude, M.J. and Petley, D.N. (2018), "Global fatal landslide occurrence from 2004 to 2016", *Nat. Hazard. Earth Syst. Sci*., **18**(8), 2161-2181. https://doi.org/10.5194/nhess-18-2161-2018.

Genuchten, M.T.V. (1980), "A closed-form equation for predicting the hydraulic conductivity of unsaturated soils", *Soil Sci. Soc. Am. J*., **44**(5), 892-898. https://doi.org/10.2136/sssaj1980.03615995004400050002x.

GEO-SLOPE International Ltd (2007a), Seepage modeling with SEEP/W 2007: an engineering methodology, user's guide. GEO-SLOPE International Ltd, Calgary.

GEO-SLOPE International Ltd (2007b), Stress–deformation modeling with SIGMA/W 2007 version: an engineering methodology. GEO-SLOPE International Ltd, Calgary.

Guo, J., Yi, S., Yin, Y., Cui, Y., Qin, M., Li, T. and Wang, C. (2020), "The effect of topography on landslide kinematics: a case study of the Jichang town landslide in Guizhou, China", *Landslides*, **17**, 959-973. https://doi.org/10.1007/s10346-019-01339-9.

Han, Z.J., He, Y.L., An, Y.F. and Li, C.Y. (2009), "A new seismotectonic belt: features of the latest structural deformation style in the Mabian seismotectonic zone", *Acta Geologica Sinica*, **83**, 218-229. (In Chinese)

He, K., Ma, G., Hu, X., Luo, G., Mei, X., Liu, B. and He, X. (2019), "Characteristics and mechanisms of coupled road and rainfall-induced landslide in Sichuan China", *Geomatics, Nat. Hazard. Risk*, **10**(1), 2313-2329. https://doi.org/10.1080/19475705.2019.1694230.

He, K., Ma, G. and Hu, X. (2021a), "Formation mechanisms and evolution model of the tectonic-related ancient giant basalt landslide in Yanyuan County, China", *Nat. Hazards*, **106**, 2575-2597. https://doi.org/10.1007/s11069-021-04555-6.

He, K., Ma, G., Hu, X. and Liu, B. (2021b), "Failure mechanism and stability analysis of a reactivated landslide occurrence in Yanyuan City, China", *Landslide*, **18**(3), 1097-1114. https://doi.org/10.1007/s10346-020-01571-8.

He, K., Liu, B. and Hu, X. (2021c), "Preliminary reports of a catastrophic landslide occurred on August 21, 2020, in Hanyuan County, Sichuan Province, China", *Landslides*, **18**(1), 503-507. https://doi.org/10.1007/s10346-020-01566-5.

Hu, X., Zhang, M., Sun, M., Huang, K. and Song, Y. (2013), "Deformation characteristics and failure mode of the Zhujiadian landslide in the Three Gorges Reservoir, China', *Bull. Eng. Geol. Environ.*, **74**(1), 1-12. https://doi.org/10.1007/s10064-013-0552-x.

Huang, R. (2009), "Some catastrophic landslides since the Twentieth Century in the southwest of China", *Landslides*, **6**(1), 69-81. https://doi.org/10.1007/s10346-009-0142-y.

Kainthola, A., Singh, P.K. and Singh, T.N. (2015), "Stability investigation of road cut slope in basaltic rockmass, Mahabaleshwar, India", *Geosci. Frontiers*, **6**(6), 837-845. https://doi.org/10.1016/j.gsf.2014.03.002.

Kang, G.C., Song, Y.S. and Kim, T.H. (2009), "Behavior and stability of a large-scale cut slope considering reinforcement stages", *Landslides*, **6**(3), 263-272. https://doi.org/10.1007/s10346-009-0164-5.

Li, H.B., Xu, Y.R., Zhou, J.W., Wang, X.K., Yamagishi, H. and Dou, J. (2020), "Preliminary analyses of a catastrophic landslide occurred on July 23, 2019, in Guizhou Province, China", *Landslides*. **17**, 719-724. https://doi.org/10.1007/s10346-019-01334-0.

Lin, J., (1985), "Spatial and temporal distribution of Permian basalts and their geological characteristics in three provinces in southwest China", *Chinese Science Bulletin*, **30**(12), 929-935. (In Chinese)

Lin, F., Wu, L. Z., Huang, R. Q., Zhang, H. (2017), Formation and characteristics of the Xiaoba landslide in Fuquan, Guizhou, China. *Landslides*, **15**(4), 669–681. https://doi.org/10.1007/s10346-017-0897-5.

Liu, B., Hu, X., He, K., He, S., Shi, H. and Liu, D. (2020), "The starting mechanism and movement process of the coseismic rockslide: A case study of the Laoyingyan rockslide induced by the "5.12" Wenchuan earthquake", *J. Mountain Sci.*, **17**(5), 1188-1205. https://doi.org/10.1007/s11629-019-5775-2.

Liu, B., He, K., Han, M., Hu, X., Wu, T., Wu, M. and Ma, G. (2021), "Dynamic process simulation of the Xiaogangjian rockslide occurred in shattered mountain based on 3DEC and DFN", *Comput. Geotech.*, **134**, 104122. https://doi.org/10.1016/j.compgeo.2021.104122.

Liu, N.N., Liu, W.L. and Wu, D.C. (2006), "A thrust fault in a hydropower plant reservoir region in the southwest China", *J. Eng. Geol.*, **14**(1), 13-17. (in Chinese).

Luo, G., Hu, X., Bowman, E.T. and Liang, J. (2017), "Stability evaluation and prediction of the Dongla reactivated ancient landslide as well as emergency mitigation for the Dongla Bridge", *Landslides*, **14**, 1403–1418. https://doi.org/10.1007/s10346-017-0796-9.

Ma, G., Hu, X., Yin, Y., Luo, G. and Pan, Y. (2018), "Failure mechanisms and development of catastrophic rockslides triggered by precipitation and open-pit mining in Emei, Sichuan, China", *Landslides*, **15**, 1401-1414. https://doi.org/10.1007/s10346-018-0981-5.

Ma, G., Rezania, M. and Mousavi, N.M. (2021a), "Effects of spatial auto-correlation structure for friction angle on runout distance in heterogeneous sand collapse", *Transportation Geotechnics*, https://doi.org/10.1016/j.trgeo.2021.100705.

Ma, G., Rezania, M., Mousavi, N.M. and Hu, X. (2021b), "Uncertainty quantification of landslide runout motion considering soil interdependent anisotropy and fabric orientation", *Landslides*, (Accepted)

Ma, G., Rezania, M. and Mousavi, N.M. (2021c), "Stochastic assessment of landslide influence zone by material point method and generalized geotechnical random field theory", *Int. J. Geomech.*, (Accepted)

Morgenstern, N.R. and Price, V.E. (1965), "Analysis of stability of general slip surfaces", *Geotechnique*, **15**, 79-93.

Nguyen, L.C., Tien, P.V. and Do, T.N. (2019), "Deep-seated rainfall-induced landslides on a new expressway: a case study in Vietnam", *Landslides*. **17**, 395-407. https://doi.org/10.1007/s10346-019-01293-6.

Nguyen, T.S., Likitlersuang, S., Ohtsu, H. and Kitaoka, T. (2017), "Influence of the spatial variability of shear strength parameters on rainfall induced landslides: a case study of sandstone slope in Japan", *Arabian J. Geosci*., **10**(16), 369. https://doi.org/10.1007/s12517-017-3158-y.

Nguyen, T.S. and Likitlersuang, S. (2019), "Reliability analysis of unsaturated soil slope stability under infiltration considering hydraulic and shear strength parameters", *Bull. Eng. Geol. Environ.*, **78**(8), 5727-5743. https://doi.org/10.1007/s10064-019-01513-2.

Peng, J., Wang, S., Wang, Q., Zhuang, J., Huang, W., Zhu, X. and Ma, P. (2018), "Distribution and genetic types of loess landlisdes in China", *J. Asian Earth Sci.*, **170**, 329-350. https://doi.org/10.1016/j.jseaes.2018.11.015.

Ren, Z., Wang, K., Yang, K., Zhou, Z.H., Tang, Y.J., Tian, L. and Xu, Z.M. (2018), "The grain size distribution and composition of the Touzhai rock avalanche deposit in Yunnan, China", *Eng. Geol.*, **234**, 97-111. https://doi.org/10.1016/j.enggeo.2018.01.007.

Schweiger, H.F., Fabris, C., Ausweger, G. and Hauser, L. (2018),

"Examples of successful numerical modelling of complex geotechnical problems", *Innov. Infrastruct. Solut.*, **4**(1), 2. https://doi.org/10.1007/s41062-018-0189-5.

Shen, T., Wang, Y., Huang, Z., Li, J., Zhang, X., Cao, W. and Gu, J. (2019), "Formation mechanism and movement processes of the Aizigou paleolandslide, Jinsha River, China", *Landslides*, **16**(2), 409-424. https://doi.org/10.1007/s10346-018-1082-1.

Wang, J.J., Liang, Y., Zhang, H.P., Wu, Y. and Lin, X. (2013), "A loess landslide induced by excavation and rainfall", *Landslides*, **11**(1), 141-152. https://doi.org/10.1007/s10346-013-0418-0.

Wang, M., Ma, G. and Wang, F. (2021), "Numerically investigation on blast-induced wave propagation in catastrophic large-scale bedding rockslide", *Landslides*, **18**(1), 785-797. https://doi.org/10.1007/s10346-020-01537-w.

Wen, B., Wang, S., Wang, E. and Zhang, J. (2004), "Characteristics of rapid giant landslides in China", *Landslides*, **1**(4), 247-261. https://doi.org/10.1007/s10346-004-0022-4.

Xing, A., Wang, G., Yin, Y., Tang, C., Xu, Z. and Li, W. (2016), "Investigation and dynamic analysis of a catastrophic rock avalanche on September 23, 1991, Zhaotong, China", *Landslides*, **13**(5), 1035-1047. https://doi.org/10.1007/s10346-015-0617-y.

Xu, Q., Fan, X. and Dong, X. (2011), "Characteristics and formation mechanism of a catastrophic rainfall–induced rock avalanche–mud flow in Sichuan, China, 2010", *Landslides*, **9**(1), 143-154. https://doi.org/10.1007/s10346-011-0278-4.

Xu, Y., Chung, S.L., Jahn, B.M. and Wu, G. (2001), "Petrologic and geochemical constraints on the petrogenesis of Permian–Triassic Emeishan flood basalts in southwestern China. Lithos", **58**(3-4), 145-168. https://doi.org/10.1016/S0024-4937(01)00055-X.

Xue, D., Li, T., Zhang, S., Ma, C., Gao, M. and Liu, J. (2018), "Failure mechanism and stabilization of a basalt rock slide with weak layers", *Eng. Geol.*, **233**, 213-224. https://doi.org/10.1016/j.enggeo.2017.12.005.

Zhang, S., Yin, Y., Hu, X., Wang, W., Zhu, S., Zhang, N. and Cao, S. (2020), "Initiation mechanism of the Baige landslide on the upper reaches of the Jinsha River, China", *Landslides*, **17**(12), 2865-2877. https://doi.org/10.1007/s10346-020-01495-3.

Zhang, Y., Luo, Y. and Yang, C. (1988), *Panxi rift region*. Geology Press, Beijing, China.

CC